

Successive spin reorientations and rare earth ordering in $\text{Nd}_{0.5}\text{Dy}_{0.5}\text{FeO}_3$: Experimental and *ab initio* investigations

Ankita Singh,^{1,*} Sarita Rajput,^{1,*} Padmanabhan Balasubramanian^{2,*}, M. Anas¹, Françoise Damay,³ C. M. N. Kumar^{4,5}, Gaku Eguchi,⁴ A. Jain^{6,7}, S. M. Yusuf^{6,7}, T. Maitra,¹ and V. K. Malik^{1,†}

¹*Department of Physics, Indian Institute of Technology Roorkee, Roorkee 247 667, India*

²*Graphic Era University, Dehradun 248002, India*


³*Laboratoire Léon Brillouin, CEA-CNRS, CEA/Saclay, 91191 Gif sur Yvette, France*

⁴*Institute of Solid State Physics, Vienna University of Technology, Wiedner Hauptstr. 8-10/138, 1040 Vienna, Austria*

⁵*AGH University of Science and Technology, Faculty of Physics and Applied Computer Science, 30-059 Kraków, Poland*

⁶*Solid State Physics Division, Bhabha Atomic Research Center, Mumbai, 400 085, India*

⁷*Homi Bhabha National Institute, Anushaktinagar, Mumbai 400 094, India*

 (Received 29 June 2020; revised 9 September 2020; accepted 9 September 2020; published 21 October 2020)

In the present paper, the magnetic structure and spin reorientation of mixed rare-earth orthoferrite $\text{Nd}_{0.5}\text{Dy}_{0.5}\text{FeO}_3$ have been investigated. At room temperature, our neutron-diffraction measurements reveal that the magnetic structure of Fe^{3+} spins in $\text{Nd}_{0.5}\text{Dy}_{0.5}\text{FeO}_3$ belongs to Γ_4 irreducible representation (G_x, F_z) as observed in both parent compounds (NdFeO_3 and DyFeO_3). The neutron-diffraction study also confirms the presence of a spin-reorientation transition where the magnetic structure of Fe^{3+} spins changes from Γ_4 to $\Gamma_2(F_x, G_z)$ representation between 75 and 20 K while maintaining a G-type antiferromagnetic configuration. Such a gradual spin reorientation is unusual since the large single ion anisotropy of Dy^{3+} ions is expected to cause an abrupt $\Gamma_4 \rightarrow \Gamma_1(G_y)$ rotation of the Fe^{3+} spins. At 10 K, the Fe^{3+} magnetic structure is represented by $\Gamma_2(F_x, G_z)$. Unexpectedly, the Γ_4 structure of Fe^{3+} spins re-emerges below 10 K, which also coincides with the development of rare-earth ($\text{Nd}^{3+}/\text{Dy}^{3+}$) magnetic ordering having c_y^R configuration. Such re-emergence of a magnetic structure has been a rare phenomenon in orthoferrites. The absence of a second-order phase transition in rare-earth ordering, interpreted from heat capacity data, suggests the prominent role of $\text{Nd}^{3+}-\text{Fe}^{3+}$ and $\text{Nd}^{3+}-\text{Dy}^{3+}$ exchange interactions. These interactions suppress the independent rare-earth magnetic ordering observed in both parent compounds due to $\text{Nd}^{3+}/\text{Dy}^{3+}-\text{Nd}^{3+}/\text{Dy}^{3+}$ exchange interactions. Our density-functional-theory calculations including Coulomb correlation and spin-orbit interaction effects (DFT+ U +SO) reveal that the C-type arrangement of rare-earth ions ($\text{Nd}^{3+}/\text{Dy}^{3+}$), with $\Gamma_2(F_x, G_z)$ configuration for Fe^{3+} moments, is energetically very close to a phase with the same rare-earth magnetic ordering but $\Gamma_4(G_x, F_z)$ configuration of Fe^{3+} spins. Further, the $\text{Nd}^{3+}-\text{Fe}^{3+}$ and $\text{Nd}^{3+}-\text{Dy}^{3+}$ exchange interactions are observed to play significant roles in the complex Fe^{3+} spin reorientation with the re-emergence of Γ_4 at low temperature. Consistent with the experimental observations, our calculations established the mixed phase (Γ_2 and Γ_4) to be the magnetic ground state of Fe^{3+} moments.

DOI: [10.1103/PhysRevB.102.144432](https://doi.org/10.1103/PhysRevB.102.144432)

I. INTRODUCTION

Rare-earth orthoferrites $R\text{FeO}_3$ ($R = \text{La}, \text{Nd}, \text{Dy}, \dots$) have been extensively studied for their potential multiferroicity, magnetoelectric effects, and other functional properties like ultrafast optical control of spins [1–7]. The orthoferrites belong to the family of perovskites and crystallize in the orthorhombic space group $Pbnm$, which is similar to manganites [8]. In comparison to highly distorted MnO_6 octahedra of the manganites, FeO_6 octahedra of the orthoferrites show least distortion with nearly equal Fe–O bond lengths at room temperature [8–10].

Due to strong isotropic exchange interactions between the Fe^{3+} spins, the orthoferrites have a relatively high Néel temperature of $T_{N1} \sim 700$ K, below which the Fe^{3+} spins order in G-type antiferromagnetic configuration expressed as $\Gamma_4(G_x, F_z)$ irreducible representation [11]. Here, G_x represents G-type antiferromagnetic ordering of Fe^{3+} spins with moment direction aligned along the crystallographic a direction, which is the easy anisotropy axis, and F_z corresponds to the weak ferromagnetic component arising from the canting of the Fe^{3+} spins due to Dzyaloshinskii-Moriya interactions.

Temperature-induced spin reorientation of Fe^{3+} moments is an essential characteristic of rare-earth orthoferrites except when R^{3+} is a nonmagnetic rare-earth ion (e.g., La^{3+} , Eu^{3+} , and Y^{3+}). Absence of spin reorientation in nonmagnetic rare-earth orthoferrites confirms that the anisotropic $\text{Fe}^{3+}-\text{Fe}^{3+}$ exchange interactions (antisymmetric and anisotropic symmetric) do not play any role in observed spin reorientation

*These authors contributed equally to this work.

†vivek.malik@ph.iit.ac.in

of the orthoferrites. Like $\text{Fe}^{3+}-\text{Fe}^{3+}$, $R^{3+}-\text{Fe}^{3+}$ exchange interaction also consists of the isotropic, antisymmetric, and anisotropic-symmetric parts. Weak ferromagnetic component (F_z) of Fe^{3+} spins polarizes R^{3+} moments (f_z^R) through isotropic exchange interaction between R^{3+} and Fe^{3+} . This isotropic exchange interaction does not play any role in spin reorientation. As temperature decreases, the polarization of R^{3+} moments increases. Antisymmetric and anisotropic-symmetric parts of exchange interactions between R^{3+} and Fe^{3+} ions produce two effective fields, $+H_z$, $-H_z$, which act perpendicularly on the Fe^{3+} moments aligned along positive and negative a directions, respectively. As a result, the easy axis of Fe^{3+} spins undergo spin reorientation from the a to c axis in the ac plane while having a G -type antiferromagnetic configuration [11,12]. In general, the orthoferrites show either a gradual rotation to the c axis with temperature as seen in $R\text{FeO}_3$ ($R = \text{Nd, Tb, Er}$) [13,14] or an abrupt one near 50 K as observed in DyFeO_3 [11,15].

Among the orthoferrites, the most studied compound NdFeO_3 has a Néel temperature (T_{N1}) of 690 K [10]. Below T_{N1} , Fe^{3+} magnetic moments order in antiferromagnetic configuration and the magnetic structure of the Fe^{3+} sublattice is represented by Γ_4 (G_x, F_z) [13]. As the temperature is reduced below 200 K, the Fe^{3+} spins continuously rotate in the ac plane between 200 K and 105 K, thereby resulting in a Γ_2 (G_z, F_x) magnetic structure below 105 K. Recent terahertz spectroscopy studies on single crystals of NdFeO_3 reveal a correlation between the gap in spin-wave dispersion and the changes in magnetic anisotropy of the system in the spin-reorientation region [16]. Below 25 K, an additional magnetic Bragg peak (100), corresponding to the Γ_2 (c_y^R, f_y^R) representation, develops in neutron diffraction, indicating polarization of Nd^{3+} magnetic moments [17]. $\text{Nd}^{3+}-\text{Fe}^{3+}$ exchange interaction is responsible for inducing such a polarization in Nd^{3+} magnetic moments. The weak ferromagnetic moments (f_x^R) associated with Nd^{3+} polarization are antiparallel to the weak ferromagnetic moments of Fe^{3+} (F_x) and compensate each other at 8 K. The ordering of Nd^{3+} and Fe^{3+} moments are compatible with each other from the group theory. Below $T_{\text{N2}} = 1.05$ K, the $\text{Nd}^{3+}-\text{Nd}^{3+}$ interactions give rise to a proper long-range independent G -type antiferromagnetic ordering of Nd^{3+} moments [17]. The observation of such a long-range antiferromagnetic ordering is confirmed by observation of a sharp peak in specific heat data which is superimposed on the low-temperature tail of the Schottky anomaly [18,19].

The most intriguing orthoferrite happens to be DyFeO_3 . Though isostructural with NdFeO_3 , the degree of structural distortion in DyFeO_3 is greater. Like all orthoferrites, the Fe^{3+} spins of DyFeO_3 also order in antiferromagnetic configuration expressed by Γ_4 (G_x, F_z) representation below T_{N1} (~ 650 K) [20]. However, near 50 K, an abrupt spin reorientation occurs; as a result, the magnetic structure changes from Γ_4 (G_x, F_z) to Γ_1 (G_y) representation, which does not have any ferromagnetic component. This is also known as a Morin transition. The Γ_1 (G_y) structure persists till the lowest temperatures at zero field [21]. Below $T_{\text{N2}} \sim 4$ K, a long-range independent antiferromagnetic ordering of Dy^{3+} moments is observed with the Γ_5 (g_x^R, a_y^R) configuration, making an angle of 33° with the

b axis while the moments are confined to the ab plane. The studies on similar compounds, viz., DyAlO_3 and DyScO_3 , have also shown that the Dy^{3+} moments order in the same Γ_5 (g_x^R, a_y^R) representation below 3.5 K [22,23]. This type of magnetic ordering is mainly dictated by the $\text{Dy}^{3+}-\text{Dy}^{3+}$ exchange interactions. Studies have thus revealed that the strong Dy^{3+} single ion anisotropy determines the ground-state magnetic properties [22,23]. Recent reports suggest that below T_{N2} , the Fe^{3+} spins orient into a different magnetic structure due to $\text{Dy}^{3+}-\text{Fe}^{3+}$ interaction [24]. In DyFeO_3 , the Γ_5 structure is not symmetry compatible with Γ_1 . The overall reduction in symmetry due to the Dy^{3+} ordering results in a linear magnetoelectric effect [12]. A large ferroelectric polarization is also observed due to the weak ferromagnetic ordering induced by the magnetic field along the c axis of the DyFeO_3 crystals [1].

$R^{3+}-R^{3+}$ is the weakest among $\text{Fe}^{3+}-\text{Fe}^{3+}$, $R^{3+}-\text{Fe}^{3+}$, and $R^{3+}-R^{3+}$ exchange interactions and is responsible for antiferromagnetic ordering of rare-earth ions below T_{N2} . The effective moments on the R^{3+} ion are determined by the local crystal electric field (CEF) effects which reduce the free ion moment and induce a magnetocrystalline anisotropy. The magnetization of the rare earth ions is determined by the lowest energy CEF level. Due to the presence of odd number of electrons, Nd^{3+} and Dy^{3+} are Kramer's ions having Kramer's doublet as a ground state. Both ions can be represented by an effective $S = 1/2$ system with an anisotropic \mathbf{g} tensor at liquid helium temperature. All the effects of the crystalline field are thus incorporated in the \mathbf{g} tensor. In this scenario, the $R^{3+}-\text{Fe}^{3+}$ and $R^{3+}-R^{3+}$ exchange interactions are considered as effective exchange fields acting on the $S = 1/2$ spins through the effective \mathbf{g} tensor which results in splitting of the Kramer's doublet. At liquid helium temperature, the magnetization of $R\text{FeO}_3$ is predominantly affected by splitting of the doublet by $R^{3+}-\text{Fe}^{3+}$ and $R^{3+}-R^{3+}$ exchange interactions.

Magnetic anisotropic behavior of rare-earth ions in $R\text{FeO}_3$ can be explained in terms of the effective \mathbf{g} tensor. In case of Nd, the \mathbf{g} tensor is nearly isotropic with smaller values [25]. However, the \mathbf{g} tensor of the Dy^{3+} is highly anisotropic with a large value in the ab plane and negligible in the c direction [22]. The anisotropic behavior of Dy^{3+} ions have already been studied from optical Zeeman effect and magnetization measurements [23,26]. In the monoclinic crystal field, the ground state of Dy^{3+} splits into a series of eight doublets [22]. Due to low symmetry, there exists only an ab mirror plane, by which the Dy^{3+} moments can lie either in the plane or perpendicular to it. In the DyMO_3 ($M = \text{Al, Sc, Fe, } \dots$) compounds, the Dy^{3+} moments remain in the ab plane with an angle ϕ (28° to 38°) with respect to the b axis [22,23]. This direction can thus be considered as axis of quantization, z' . Thus, by the anisotropy of the CEF, the Dy^{3+} moments can be considered as Ising spins in the z' direction in all the DyMO_3 compounds.

Substitution at the R or Fe site provides the possibility of achieving the tunability of desired electrical and magnetic properties in orthoferrites. For example, 50% substitution of M (Co, Rh, Ir, Mo) at the Fe site and doping of divalent ions (e.g., Sr^{2+}) at the trivalent La site of LaFeO_3 foster B-site cationic ordering and the resultant compound is represented

by $\text{La}_{2-x}\text{Sr}_x\text{FeMO}_6$ having a double perovskite structure. Magnetic ordering of these substituted compounds may lead to realization of ferromagnetic, antiferromagnetic, and spin-glass ground states [27–32]. $\text{Sr}_2\text{FeCoO}_6$ exhibits a glassy state as opposed to $\text{La}_2\text{FeCoO}_6$, which remains antiferromagnetic despite the prediction of a ferromagnetic ground state [27,31,33]. Positive exchange bias was reported in case of $\text{LaCr}_{0.5}\text{Fe}_{0.5}\text{O}_3$ [34]. With the substitution, we wish to observe a change in the magnetic structure of Fe^{3+} spins, which we expected to be influenced by both the rare-earth as well as the transition-metal ion. Additionally, exchange interactions and magnetic anisotropies in RFeO_3 can be tuned to observe successive spin reorientations which can be exploited for magnetic switching at different temperature regimes. For instance, substitution of Fe by Mn in NdFeO_3 affects the spin reorientation such that the Γ_1 magnetic structure occurs in a wide temperature range suppressing the Γ_4 magnetic structure [35]. In $\text{YFe}_{1-x}\text{Mn}_x\text{O}_3$, ferroelectricity and magnetodielectric effects are observed [7]. Similarly, the presence of two rare-earth ions at the R site also yield an interesting set of properties. For instance, an enhanced ferroelectricity is observed in $\text{Dy}_{0.7}\text{Pr}_{0.3}\text{FeO}_3$ [36]. In $\text{Dy}_{0.5}\text{Ho}_{0.5}\text{FeO}_3$, though the Morin transition occurs at 49 K, an additional $\Gamma_1 \rightarrow \Gamma_2$ transition occurs at 26 K [37]. Interestingly, in $\text{Dy}_{0.5}\text{Pr}_{0.5}\text{FeO}_3$, the Morin transition occurs at 75 K itself, followed by an additional reorientation at a lower temperature [38]. Thus the Morin transition seems unaffected by Ho^{3+} , while greatly enhanced by Pr^{3+} ions, even though the low-temperature rare-earth ordering is affected. Surprisingly, $\Gamma_4 \rightarrow \Gamma_2$ reorientation occurs at much lower temperatures (10–6 K) in PrFeO_3 [39]. Thus, the nature of exchange interactions between the two different rare-earth ions and also with that of Fe^{3+} can lead to a behavior different from that of both the parent compounds.

In view of this, it would be interesting to observe behavior of the compound $\text{Nd}_{0.5}\text{Dy}_{0.5}\text{FeO}_3$ (NDFO). With Nd^{3+} , being a Kramer's ion similar to Dy^{3+} , the result can be more complex. In the present paper, the magnetic and thermodynamic properties of NDFO have been investigated using the bulk magnetization, neutron-diffraction, and specific-heat techniques. In addition, density-functional-theory (DFT) calculations have been used to establish the ground-state magnetic structure of NDFO as well as to qualitatively understand the underlying mechanism of spin reorientation and the nature of rare-earth ordering. Our results show that the $\text{Nd}^{3+}-\text{Fe}^{3+}$ interactions result in $\Gamma_4 \rightarrow \Gamma_2$ reorientation at relatively higher temperatures (75 K) in comparison to the Morin transition. The stronger $\text{Dy}^{3+}-\text{Dy}^{3+}$ interactions which result in rare-earth ordering and the strong single ion anisotropy of Dy^{3+} can compete with the $\text{Nd}^{3+}-\text{Fe}^{3+}$ exchange interactions, thereby affecting the Morin transition and also the rare-earth ordering. Surprisingly, the presence of 50% Nd completely suppresses the Morin transition, yielding a successive twofold spin reorientation ($\Gamma_4 \rightarrow \Gamma_2 \rightarrow \Gamma_4$) of the Fe^{3+} spins. Also, the independent rare-earth ordering completely vanishes even down to 0.4 K as seen in our specific-heat studies. Rather, the $\text{Nd}^{3+}/\text{Dy}^{3+}$ moments order by means of induced polarization by $\text{R}^{3+}-\text{Fe}^{3+}$ interactions. Also, the absence of any magnetoelectric effect as predicted by symmetry is confirmed by dielectric studies under an external magnetic field.

II. METHODS

A. Experimental

Powder sample of NDFO was synthesized using solid-state-reaction method. Nd_2O_3 , Dy_2O_3 , and Fe_2O_3 were weighed according to appropriate stoichiometry and ground in an agate mortar for 12 hours. The sample was calcined and sintered consecutively at 1200°C, 1300°C, and 1400°C for 24 hours with intermedieate grindings. Structural phase of the sample was identified using a Bruker D8 two circle x-ray diffractometer at Cu K_α wavelength. Bulk magnetization measurements were performed using a superconducting quantum user interface device magnetometer of Quantum Design Inc.'s magnetic measurement system-XL and vibrating sample magnetometer option of Quantum Design Inc.'s Dynacool physical properties measurement system (PPMS). Temperature-dependent zero field-cooled (ZFC) and field-cooled (FC) measurements were carried out to identify the different magnetic transitions and their respective transition temperatures. Field variation of magnetization was carried out at various temperatures between 300 and 5 K. Heat-capacity measurements were carried out using the heat-capacity option of Quantum Design Inc.'s PPMS for temperature range of 2–200 K and ^3He refrigerator for temperature range of 0.4–20 K. Magnetodielectric measurements were carried out using a custom design probe for PPMS sample chamber.

Neutron-diffraction studies in zero magnetic field were carried out at various temperatures in the range of 1.5–300 K to identify the crystal as well as magnetic structure and their variations as a function of temperature. The neutron-diffraction measurements were performed at powder diffractometers G 4-1 ($\lambda = 2.4206 \text{ \AA}$) of Laboratoire Léon Brillouin, Saclay, France. The diffraction data were analyzed using FULLPROF [40] suite of programs utilizing the Rietveld refinement method [41]. Magnetic structure was determined using the irreducible representations from BasIreps [42] and refined using FULLPROF.

B. Theoretical

Electronic structure of NDFO was obtained using the projector-augmented wave pseudopotential and a plane-wave-basis method within the DFT framework as implemented in the Vienna Ab-Initio Simulation Program [43]. Calculations were performed within Perdew-Burke-Ernzerhof generalized gradient approximation (PBE-GGA) [44] and GGA+ U approximation [45]. The structure was relaxed keeping the Nd/Dy $4f$ states as frozen in the core. Ionic positions were relaxed until the forces on the ions are less than 0.1 meV \AA^{-1} . For the subsequent self-consistent calculations, the Nd/Dy $4f$ states were treated as valence states. The (Fe) $3d$, $4s$, O $2s$, $2p$ and Nd $5p$, $5d$, $6s$ states were treated as valence states. An energy cutoff of 450 eV was used for the plane-wave-basis set while a $6 \times 6 \times 6$ Monkhorst-Pack k -mesh centered at the Γ point was used for performing the Brillouin zone integrations.

III. EXPERIMENTAL RESULTS

A. Structural characterization

Figure 1 shows the room-temperature powder x-ray diffraction pattern of the NDFO. The compound crystallizes

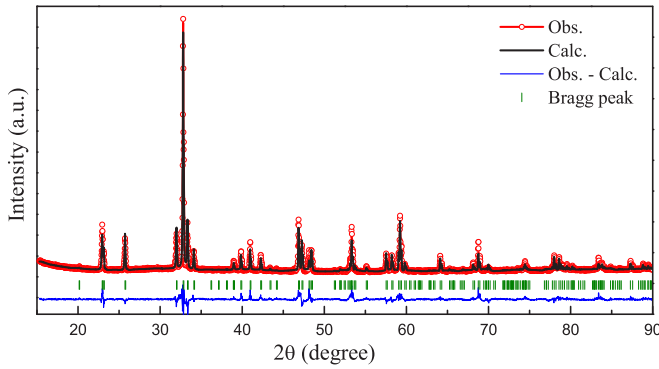


FIG. 1. Observed and simulated x-ray diffraction pattern of NDFO at 300 K, refined using $Pbnm$ space group.

in the orthorhombic $Pbnm$ space group. The observed x-ray diffraction pattern of NDFO shows no traces of any impurity phase.

The neutron-diffraction patterns were collected systematically at regular intervals between 1.5 K to 300 K. In Table I, the lattice constants along with Fe–O ($M = \text{Fe}$) and Nd(Dy)–O bond lengths of NDFO, obtained from the combined refinement of the x-ray and neutron diffraction data at 300 K are shown. The values of bond lengths and bond angles at 1.5 K have been obtained from the refinement of the neutron diffraction data. Three different Fe–O bond lengths correspond to the apical and in-plane bond lengths. Unlike the manganites which have highly unequal bond lengths, the orthoferrites have nearly equal Fe–O bond lengths. From Table I, we can infer that a contraction in out-of plane bond length occurs, while the in-plane bond lengths remain nearly constant with temperature.

The lattice parameters of NDFO are intermediate to the lattice parameters of both the parent compounds (NdFeO_3 and DyFeO_3) [10,15]. The ratio b/a , which increases monotonically with the atomic number of the rare earth, has a value of 1.024 in case of NdFeO_3 . In NDFO, the value of b/a is 1.040, which is closer to the value obtained for DyFeO_3 [10,15]. In Fig. 2, the temperature variation of lattice parameters and unit cell volume of NDFO is shown. Starting from 300 K, a , b , and c show a sharper and continuous decrease till 60 K. From 60 K till 30 K, b shows an increase indicating a crossover from positive to negative thermal expansion. Below 30 K, b shows

TABLE I. Structural parameters of $\text{Nd}_{0.5}\text{Dy}_{0.5}\text{FeO}_3$ obtained using combined Rietveld refinement of neutron and x-ray diffraction data at 300 K and refinement of neutron diffraction data at 1.5 K.

Parameters	300 K (neutron and x ray)	1.5 K (neutron)
$a(\text{\AA})$	5.377(2)	5.364(2)
$b(\text{\AA})$	5.597(2)	5.586(3)
$c(\text{\AA})$	7.694(4)	7.669(2)
Fe–O(1)(m) \AA	2.021(3)	1.966(4)
Fe–O(2)(l) \AA	2.040(2)	2.018(2)
Fe–O(2)(s) \AA	2.027(2)	2.037(2)

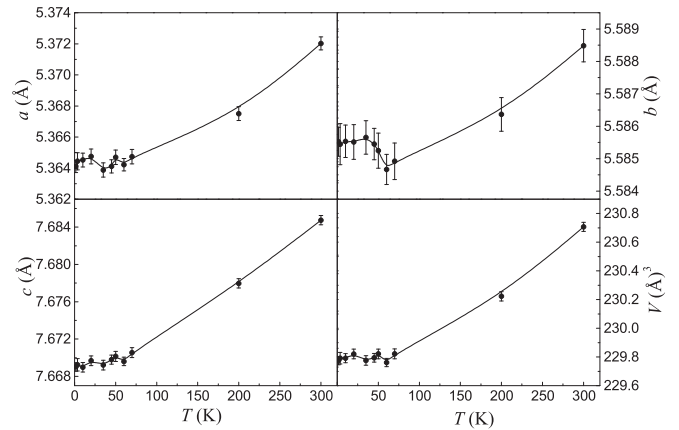


FIG. 2. Temperature variation of lattice parameters and unit cell volume of NDFO. Solid lines are guide to the eye.

a plateaulike behavior with no significant change with further decrease in temperature. Similar variation in b is also reported for NdFeO_3 [10]. However, in NdFeO_3 , the rise in b starts at 150 K itself, which is more gradual and finally converging to a plateau near 50 K. This temperature range (150–50 K) also coincides with the spin-reorientation range of NdFeO_3 . The trend reversal of b below 60 K is also accompanied by slope changes in a and c . The variation of c below 60 K is considerably smaller compared to the fluctuations in a . The slope change in b coincides with the advent of spin reorientation of the Fe^{3+} spins in NDFO, which is discussed in detail further in the subsequent sections. The variation of unit cell volume V [Fig. 2(d)] is similar to reported variation in NdFeO_3 [10]. The unit cell volume variation does not show any signs related to magnetoelastic or magnetovolume effect due to spin reorientation.

B. Magnetic properties

1. DC magnetization

As shown in Fig. 3, ZFC and FC magnetization measurements were performed from 2 K to 300 K in presence of

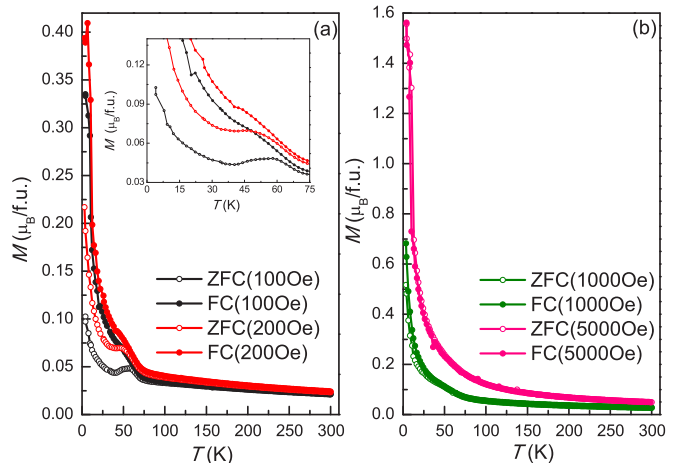


FIG. 3. ZFC-FC plots of NDFO at (a) 100 Oe and (b) 1000 and 5000 Oe.

100, 200, 500, 1000, and 5000 Oe (external magnetic field values). Both the parent compounds, NdFeO₃ and DyFeO₃, undergo transition from a paramagnetic state to a G-type antiferromagnetic state with the magnetic structure represented by $\Gamma_4(G_x, F_z)$ at 690 K and 650 K, respectively [10,20]. Thus at 300 K, NDFO is already in the antiferromagnetically ordered state with $\Gamma_4(G_x, F_z)$ structure, similar to end compounds. As shown in Fig. 3(a), a magnetic transition is observed in the ZFC-FC magnetization data below ≈ 75 K. In DyFeO₃, an abrupt spin reorientation is observed at 50 K which corresponds to $\Gamma_4 \rightarrow \Gamma_1$ transition, i.e., Morin transition. The Γ_1 representation, which corresponds to antiferromagnetic G_y magnetic structure in Bertaut notation, does not contain any net effective ferromagnetic moment. Although low-field (100 Oe and 200 Oe) ZFC measurements of NDFO show a drop in magnetization below 60 K (see Fig. 3(a)), however an increase in 100 Oe and 200 Oe FC magnetization is observed contrary to the expected behavior from Γ_1 (G_y) magnetic structure. The ZFC magnetization values also increase below 35 K during the 100 and 200 Oe ZFC measurements. As shown in Fig. 3(a), an observed bifurcation of ZFC and FC magnetization values can also be expected from a spin-glass system, but ac susceptibility measurements (not shown) on NDFO rule out the possibility of a spin glass phase. As shown in Fig. 3(b), ZFC-FC measurements were also carried out at higher magnetic fields of 1000 and 5000 Oe. With the increasing field, we see a gradual suppression of the transition below 75 K. As the temperature decreases, at a field of 5000 Oe, the ZFC as well as FC magnetization show a continuous increase without any noticeable bifurcation.

In both parent compounds (NdFeO₃ and DyFeO₃), the application of external magnetic fields have drastically different effects. In NdFeO₃, although the magnetization data under applied magnetic fields show anisotropic behavior and magnetization reversal, but an external field-induced spin reorientation is not observed [13]. However in DyFeO₃, though the Dy³⁺-Fe³⁺ exchange interactions do not affect independent ordering of both the ions, application of an external magnetic field along various crystal axes result in multiple spin reorientations. The reorientation can be spin flop as well as screw rotations, depending upon the direction of magnetic field. Thus near 77 K (well above the Morin transition), at a critical field of 4.5 T along the a direction, the Fe³⁺ spins in DyFeO₃ undergo a field-induced $\Gamma_4 \rightarrow \Gamma_2$ reorientation [21]. For field along b and c directions, the Γ_4 magnetic structure is retained and, eventually, the Morin transition is suppressed. This suggests that, in NDFO, the x component of the molecular field $\mathbf{H}_{\text{Nd-Fe}}$ can also cause the reorientation of a significant fraction of the total Fe³⁺ spins, in a manner similar to that of the applied field in DyFeO₃. Thus in NDFO, a continuous $\Gamma_4 \rightarrow \Gamma_2$ reorientation occurs below 75 K, eventually suppressing the Morin transition.

Figure 4 shows the M - H curves, measured at different temperatures. At 200 K, the magnetization is linear at higher magnetic field, along with slightly nonlinear behavior and hysteresis at lower field values as shown in the inset. The similar behavior is observed qualitatively for magnetization isotherms measured between 300 and 75 K. Below 75 K,

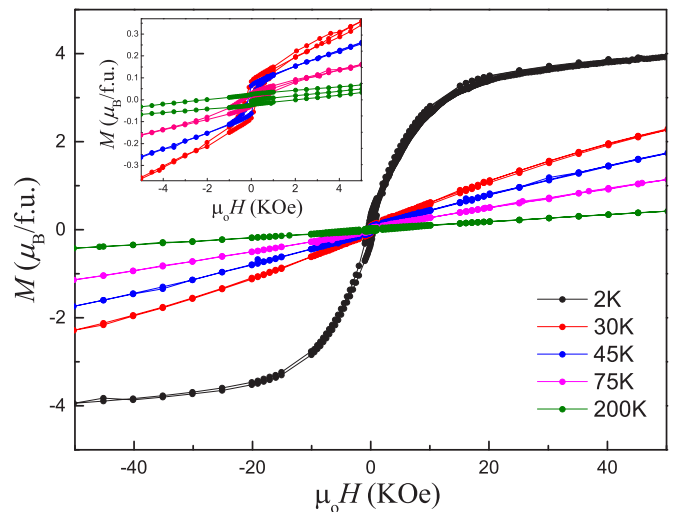


FIG. 4. M - H plots of NDFO at 200 K, 75 K, 45 K, 30 K, and 2 K.

coercivity varies significantly with a narrow hysteresis loop of the M - H isotherms. The reduction in loop width coincides with the onset of magnetic transition in ZFC-FC measurements. Below 30 K, the magnetization in M - H measurements shows a nonlinear behavior at high fields. At 2 K, the M - H isotherm shows a completely different trend qualitatively as well as quantitatively. A nearly saturation magnetization along with smaller coercivity is observed below 10 K. A large magnetization value of nearly $4 \mu_B/\text{f.u.}$ is attained at 5 T magnetic field. This can be attributed mainly to the large magnetic moment associated with the Dy³⁺ ion ($J=15/2$). At 2 K, magnetization studies on single crystals of DyFeO₃ revealed that the magnetic moment along a and b crystallographic directions attain saturation values of $4.32 \mu_B/\text{f.u.}$ and $8.59 \mu_B/\text{f.u.}$, respectively, while along the c direction it shows a linear trend and attains a smaller value of $0.71 \mu_B/\text{f.u.}$ at 5 T [24]. In our polycrystalline NdFeO₃ sample, the magnetic moment reaches a value of $1.28 \mu_B/\text{f.u.}$ in a field of 5 T at 2 K. Thus, considering the 50% substitution by Nd atoms and the polycrystalline nature of our sample, an approximate value of $2.91 \mu_B/\text{f.u.}$ for magnetization of NDFO is expected at 5 T and 2 K. This expected value of magnetic moments is much lower than the observed one (see Fig. 4), indicating a greater field-induced polarization in NDFO. Below 10 K, Dy³⁺-Nd³⁺ and Nd³⁺-Fe³⁺ exchange interactions play a crucial role in observation of higher value of magnetization induced by the rare-earth ordering/polarization [46]. The hysteresis loop parameters, viz., coercivity and retentivity at 2 K suggest a possible ordering of the rare-earth ions.

Thus, the M - T (ZFC-FC) measurements and M - H isotherms indicate the presence of a gradual spin reorientation below 75 K. The FC measurements also rule out the possibility of a Morin transition. These dc magnetization measurements infer a possibility of rare-earth (Dy³⁺/Nd³⁺) ordering at lower temperatures (< 10 K).

Magnetization measurements can not provide a conclusive evidence regarding the spin reorientation as well as rare-earth ordering. Thus, neutron diffraction measurements were carried out to understand the low temperature magnetic transitions in NDFO.

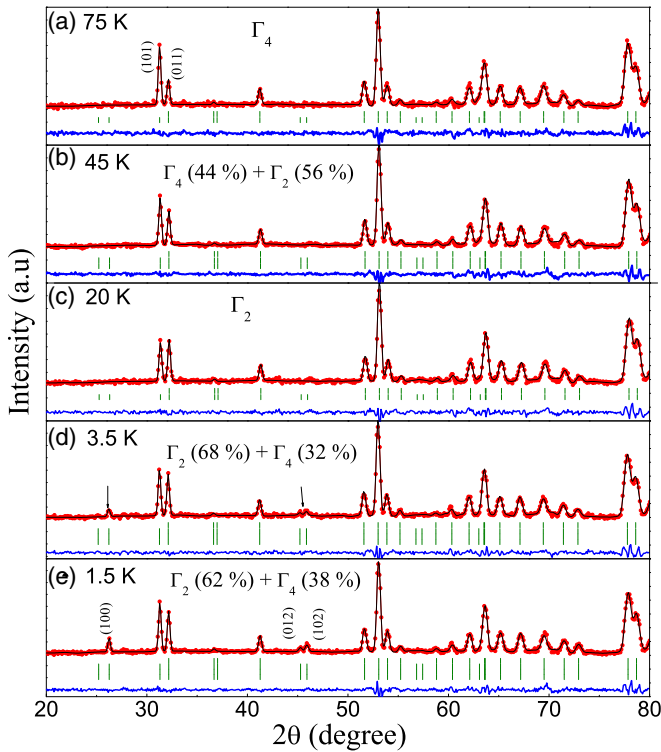


FIG. 5. Evolution of the neutron diffraction data along with refinement as a function of temperature.

2. Neutron diffraction

In this section, a systematic evolution of the NDFO magnetic structure, based on neutron-diffraction data, is discussed. To obtain the detailed configurations of Fe^{3+} and R^{3+} ($\text{Nd}^{3+}/\text{Dy}^{3+}$) magnetic moments in the unit cell, the magnetic structure has been solved from refinement of the powder neutron-diffraction patterns for temperatures between 300 and 1.5 K. The Fe atoms occupy the $4b$ Wyckoff positions, while the R atoms occupy the $4c$ sites. The magnetic ordering vector remains $k = (0, 0, 0)$ in the entire temperature range for both Fe and R atoms. Eight irreducible representations, Γ_1 to Γ_8 , exist from the symmetry analysis by Bertaut *et al.* [47]. Four out of these eight representations correspond to zero coefficients for the Fe site. Thus, only four irreducible representations Γ_1 to Γ_4 can be considered which correspond to the Shubnikov magnetic space groups, Γ_1 ($Pbnm$), Γ_2 ($Pbn'm'$), Γ_3 ($Pb'nm'$), and Γ_4 ($Pb'n'm$). Using Bertraut's notation [47], Γ_1 , Γ_2 , Γ_3 , and Γ_4 representations can be written in a simplified manner as G_y , $F_x G_z$, $C_x F_y$, and $G_x F_z$, respectively, corresponding to magnetic ordering of the Cartesian components of Fe^{3+} spins in the unit cell. Symbols G and C represent the type of antiferromagnetic ordering and F represents the ferromagnetic component due to canting of antiferromagnetically ordered Fe^{3+} spins. Subscripts to the symbol represent the directions of Fe^{3+} spins.

Figure 5 shows neutron-diffraction patterns between 75 and 1.5 K. At 300 K, the (101) and (011) magnetic peaks associated with G-type antiferromagnetic ordering of the Fe^{3+} spins are observed near $2\theta = 32^\circ$ (data not shown). A ratio of 1/3 between the intensities of (101) and (011) magnetic peaks indicates that the magnetic structure belongs

to the Γ_4 representation with a G_x ordering of the Fe^{3+} spins at 300 K which is confirmed by refinement of the data. The ratio and intensities of (101) and (011) reflections do not vary down to 75 K. The refined diffraction pattern at 75 K is shown as Fig. 5(a). Below 75 K, the ratio ($I_{(101)}/I_{(011)}$) systematically increases with decreasing the temperature, indicating a change in the magnetic moment direction without modification of the G-type magnetic structure, i.e., spin reorientation. As shown in Figs. 5(a), 5(b), and 5(c), this variation in the ratio of peak intensities persists down to 20 K, wherein the intensities of both the peaks have become almost equal ($I_{(101)}/I_{(011)} = 1$). At 20 K, the presence of magnetic ordering represented by Γ_2 irreducible representation (F_x , G_z) is evident due to equal intensities of the (011) and (101) peaks. Below 10 K, the intensity of the (101) peak again increases with respect to the (011) peak, which suggests a second spin reorientation/reoccurrence of magnetic phase ($\Gamma_2 \rightarrow \Gamma_4 + \Gamma_2$). At the lowest temperatures, viz., 3.5 and 1.5 K [Figs. 5(d) and 5(e)], three additional peaks develop at $2\theta = 25^\circ$ and 45° , which marks the rare-earth magnetic ordering.

In NDFO, from 300 K till 75 K, the magnetic structure belongs to Γ_4 representation, wherein the Fe spins are arranged in G_x -type antiferromagnetic structure with a weak ferromagnetic component (F_z) along the crystallographic c direction. From the diffraction pattern, we do not find any peak corresponding to the ferromagnetic F_z component, i.e., the (002) peak near $2\theta = 40^\circ$. The peak might be undetected due to small values of canting angle, leading to a small ferromagnetic moment of less than $0.1 \mu_B/\text{f.u.}$ which is not seen from our powder-diffraction experiments. The observed antiferromagnetic spin configuration is consistent with the established magnetic structure of the orthoferrites [10,13].

Below 60 K, the magnetic structure is best refined with the mixture of Γ_2 and Γ_4 representations, indicating the on-going process of spin reorientation. As shown in Fig. 5(b), the magnetic structure of NDFO consists of 44 % Γ_4 and 56 % Γ_2 phases at 45 K. The refinements down to 20 K clearly indicate that a gradual $\Gamma_4 \rightarrow \Gamma_2$ -type spin-reorientation takes place in NDFO, which is similar to the usual second-order spin reorientation observed in NdFeO_3 [13]. This is in contrast with the $\Gamma_4 \rightarrow \Gamma_1$ -type abrupt spin reorientation observed in DyFeO_3 [11,15]. As indicated by the equal ratio of $I_{(101)}$ and $I_{(011)}$ at 20 K, our analysis confirmed that the magnetic structure belongs entirely to the Γ_2 representation. Inclusion of Γ_4 leads to higher values of χ^2 . At 10 K and below, high-temperature magnetic phase (Γ_4) again starts to reappear and the magnetic structure belongs to a mixture of $\Gamma_2 + \Gamma_4$ representations. Interestingly, below 10 K, the volume fraction of Γ_4 increases gradually, while that of Γ_2 reduces, a trend which is reverse to the observed spin reorientation between 60–20 K. As shown in Figs. 5(d) and 5(e), this trend is visible clearly from the variation in intensities of the (101) and (011) peaks. At lowest measured temperature (1.5 K), 62 % Γ_2 and 38 % Γ_4 phases constitute the antiferromagnetic order of Fe^{3+} spins in NDFO.

At 3.5 K, the (100) magnetic peak at 25° , (012) and (102) magnetic peaks around $2\theta = 45^\circ$, pertaining to rare-earth ordering, arise due to the c_y^R -type arrangement of R^{3+} ($\text{Dy}^{3+}/\text{Nd}^{3+}$) moments which also belong to the Γ_2 representation. In NDFO, the C-type ordering of $\text{Dy}^{3+}/\text{Nd}^{3+}$

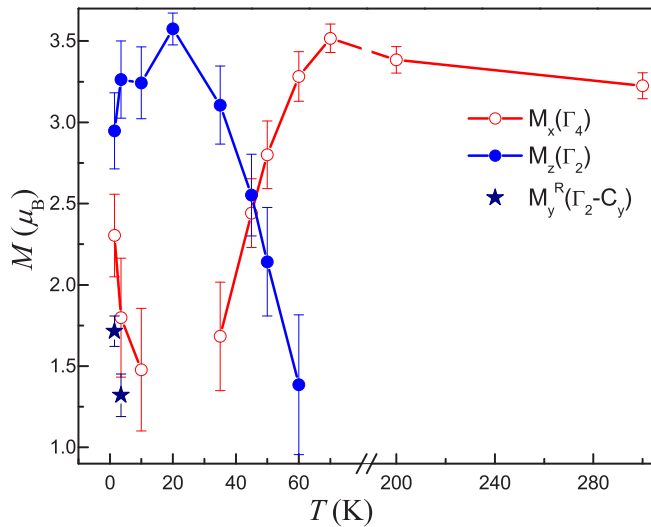


FIG. 6. Temperature variation of magnetic moments of Fe^{3+} and $\text{Nd}^{3+}/\text{Dy}^{3+}$ spins from 1.5 K to 300 K for the various representations.

moments is unusual since the $\text{Dy}^{3+}-\text{Dy}^{3+}$ interactions and strong single-ion anisotropy of the Dy^{3+} moments would have resulted in a G-type (g_x^R, a_y^R) ordering [12]. However, in NDFO, the neutron-diffraction patterns do not show a signature of G-type ordering till 1.5 K.

The temperature variation of the magnetic moments for the Fe^{3+} and R^{3+} moments for different magnetic structures is shown in Fig. 6. From 300 K till 75 K, a small increase in the magnetic moment associated with the $\Gamma_4(G_x)$ representation of Fe^{3+} spins, is observed. Below 60 K, with the onset of first spin reorientation, there is a systematic decrease in the magnetic moment along the crystallographic a direction (M_x) while, correspondingly, the magnetic moment along c direction (M_z) shows an increase. M_z attains maximum value at 20 K, conforming the presence of magnetic structure represented by Γ_2 only. At 10 K and below, the M_z magnetic moment starts to decrease, while the M_x again starts to increase. The values of total magnetic moment of Fe^{3+} is nearly $3.7 \mu_B$, which is lower than the theoretical (ionic) value $5 \mu_B$.

Such a reduction in magnetic moment can be due to the effects of covalency and the polycrystalline nature of our sample. On the other hand, the magnetic moment of $\text{Nd}^{3+}/\text{Dy}^{3+}$ is nearly $1.8 \mu_B$ at 1.5 K. This value of magnetic moment ($1.8 \mu_B$) of $\text{Nd}^{3+}/\text{Dy}^{3+}$ is twice the value of $0.9 \mu_B$ which was obtained from neutron-diffraction measurements on the single crystals of NdFeO_3 [17]. This indicates the greater polarization of the rare-earth sublattice due to $R^{3+}-\text{Fe}^{3+}$ exchange interaction, which also causes the alignment of highly anisotropic Dy^{3+} magnetic moments. As discussed in Secs. IV and V, the enhancement of the polarization and magnetic ordering of rare-earth moments are explained by calculating the strength of various exchange interaction using DFT. The schematic representation of Fe^{3+} and rare-earth ($\text{Nd}^{3+}/\text{Dy}^{3+}$) magnetic structure along with temperature-dependent successive spin reorientation is depicted in Fig. 7.

C. Heat capacity

The zero field molar heat-capacity data of NDFO have been shown in Fig. 8(a) for the temperature range from 2 to 200 K. The heat-capacity data could not identify any distinct signature associated with the spin reorientations of Fe^{3+} moments within the limit of measurement resolution. The heat-capacity measurements were extended down to 0.4 K to investigate the possible rare-earth (Nd/Dy) ordering. The molar heat capacity data over 0.4–15 K under 0 and 5 T are shown in Fig. 8(b).

To estimate the lattice contribution in the heat capacity, an isomorphous nonmagnetic compound LaGaO_3 was synthesized and its heat capacity was measured in the range 0.4–15 K. The lattice contribution for LaGaO_3 follows Debye function with effective Debye temperatures of 390 and 495 K for (La and Ga) and O atoms, respectively [48]. The lattice contribution for the heat capacity of NDFO has been estimated using the Debye function with effective Debye temperature of 495 K for oxygen atoms and 384.8 K (renormalized with the mass) for Nd/Dy and Fe atoms.

The molar heat-capacity data of NDFO, after removing the lattice contribution, have been shown in Fig. 8(c). Below 10 K, a broad peak in the heat capacity is observed at ~ 2.2 K which shifts to a higher temperature under an applied magnetic field of 5 T. The observed broad peak in NDFO could originate

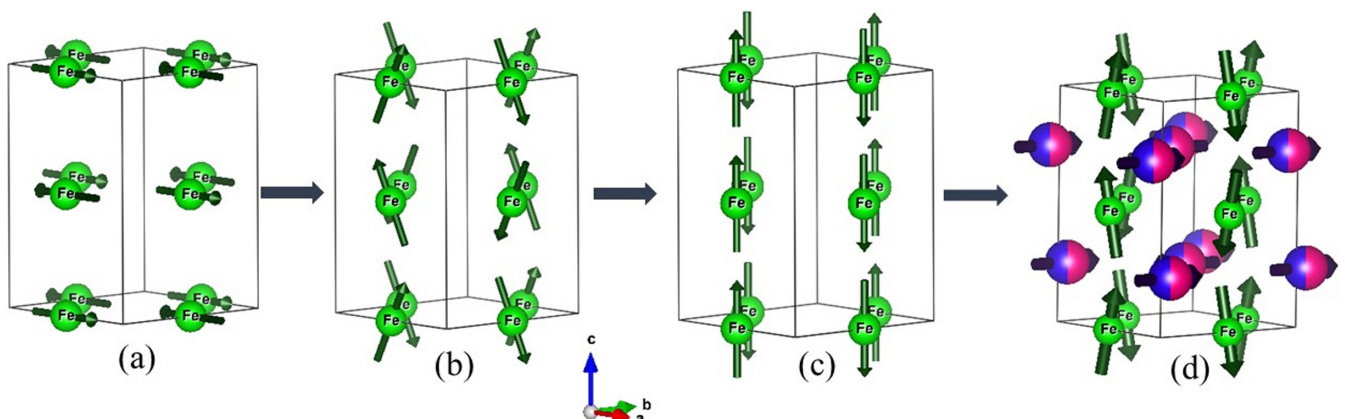


FIG. 7. Schematic representation of NDFO magnetic structure at (a) 300 K: Γ_4 (b) reorientation region at 45 K: Γ_{42} (c) at 20 K: Γ_2 and (d) 1.5 K second reorientation: Γ_{24} and ordering of Nd/Dy as C_y .

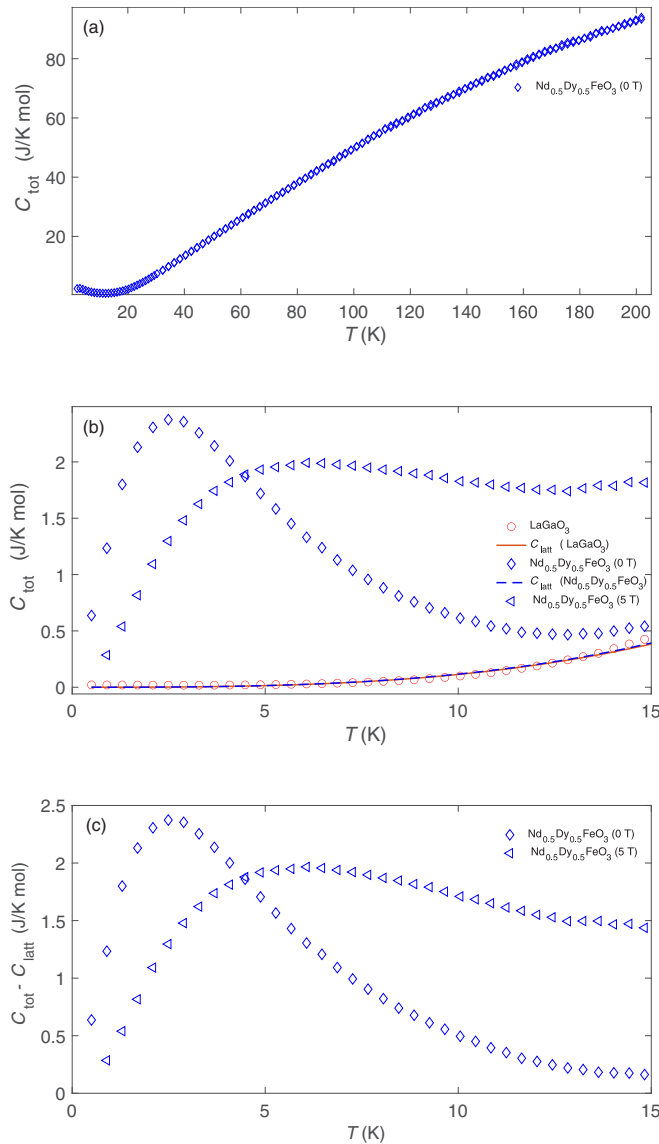


FIG. 8. (a) The molar heat capacity of NDFO measured at 0 T over 2–220 K. (b) The molar heat capacity of NDFO and nonmagnetic analog LaGaO₃ measured at 0 T over 0.4–15 K. Solid red line shows calculated lattice contribution to the molar heat capacity for LaGaO₃. Dashed blue line: Renormalized lattice contribution for NDFO. Open triangles show molar heat capacity of NDFO at 5 T over 0.4–15 K. (c) Molar heat capacity for NDFO at 0 and 5 T after subtracting the lattice contribution.

from the Schottky anomaly due to crystal-field splitting of $4f$ electronic states in Nd^{3+} and Dy^{3+} ions. We could not satisfactorily fit the observed peak and its field dependence by considering only the Schottky term associated with crystal-field splitting of Nd^{3+} and Dy^{3+} ions. This shows that the magnetic ordering of the rare earth also contributes to the observed broad peak of low temperature (<10 K) heat-capacity data. In NDFO, the presence of two Kramer's ions can cause additional complexity due to entirely different strengths of $\text{Nd}^{3+}-\text{Fe}^{3+}$ and $\text{Dy}^{3+}-\text{Fe}^{3+}$ exchange interactions which lift the degeneracy of both the doublets. In addition, the R - R

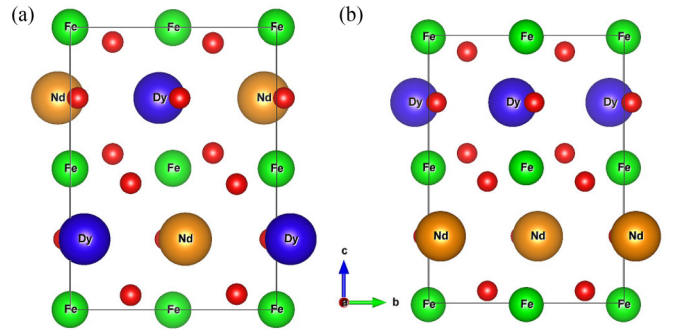


FIG. 9. Unit cells of NDFO displaying two possible arrangements of Nd and Dy ions considered in our calculations: (a) alternate, (b) layered.

exchange interactions also split the doublet in a more complex manner.

The λ -shaped anomaly associated with the second-order phase transition of rare-earth magnetic ordering is not observed till 0.4 K. The λ -shaped anomaly is seen prominently in DyFeO₃ at 4.2 K [24]. On the other hand, NdFeO₃ shows a broad Schottky peak along with a less noticeable λ anomaly superposed on the Schottky anomaly at 1.05 K [18]. Thus, as per our measurements, a distinct discontinuity (second-order transition) in heat capacity due to independent ordering of the rare earth is completely absent in NDFO. Thus, the ordering of rare-earth in NDFO is driven by the effects of molecular field due to Fe^{3+} spins, rather than independent rare-earth ordering.

IV. DFT RESULTS

To understand the complex interplay between the $\text{Nd}^{3+}/\text{Dy}^{3+}$ and Fe^{3+} magnetic moments, the ground-state magnetic order is evaluated using DFT. Since the Nd and Dy atoms occupy the same crystallographic site, their occupancies are random. However, for computational purposes, we have considered two possible arrangements of the Nd and Dy: alternate (or 111) and layered (or 001). In the alternate (111) arrangement, the Nd and Dy atoms are placed adjacent to each other. Thus, each Nd atom has six Dy atoms as nearest neighbors and vice versa. In the layered (001) arrangement, the planes of Nd and Dy atoms are alternately stacked along the c direction [35]. Figure 9 depicts these two possible arrangements: (a) alternate (111) and (b) layered (001). These two different arrangements give us scope to probe the nature of $\text{Nd}^{3+}-\text{Nd}^{3+}$, $\text{Dy}^{3+}-\text{Dy}^{3+}$, and $\text{Nd}^{3+}-\text{Dy}^{3+}$ exchange interactions. Structural relaxation of the orthorhombic unit cell with the experimental lattice parameters obtained at 1.5 K has been performed for both the possible arrangements of Nd and Dy atoms discussed above. The structure was relaxed considering the G-type magnetic ordering of the Fe^{3+} magnetic moments. The $4f$ electrons of Nd and Dy are treated as core electrons during relaxation. To obtain the ground-state magnetic ordering of Fe^{3+} and $\text{Nd}^{3+}/\text{Dy}^{3+}$ sublattices, the electronic self-consistent calculations are performed considering the effects of Coulomb correlation U for the Fe $3d$ states and Nd/Dy $4f$ states. The values of Hubbard parameters used (Coulomb correlation U and Hund's exchange J) are such

TABLE II. Relative energies (in meV) for two main antiferromagnetic orders of R^{3+} ions within GGA+ U ($U_{\text{eff}}=6$ eV at Nd/Dy and 3 eV at Fe sites) for the two different Nd/Dy arrangements.

Magnetic structure	Alternate	Layered
C-type	0	0
G-type	+55	+30

that $U_{\text{eff}} = U - J = 6.0$ eV for Nd and Dy, while for Fe, $U_{\text{eff}} = 3.0$ eV which are also used in the previous literature [49]. The self-consistent calculations are performed till an energy difference of 10^{-6} eV between successive iterations is achieved.

The ground-state magnetic structure was determined by comparing total energies of various arrangements of Fe^{3+} and $\text{Nd}^{3+}/\text{Dy}^{3+}$ magnetic moments. As the magnetic ordering of the Fe^{3+} sublattice occurs at a much higher temperature compared to that of the rare-earth ordering, we have performed calculations of collinear A-, C-, and G-type antiferromagnetic configurations along with ferromagnetic one in the absence of magnetic ordering of the rare-earth ions (i.e., we considered $4f$ electrons as core electrons for this purpose). The lowest energy in this case is obtained for G-type magnetic ordering, which is the preferred ordering of Fe^{3+} spins in all orthoferrites below the Néel temperature and above the spin reorientation transition.

To probe the rare-earth ordering, the Fe^{3+} magnetic moments are fixed as G-type in the calculations. In the case of parent compounds NdFeO_3 and DyFeO_3 , the rare-earth moments order in C- and G-type AFM, respectively [50]. Therefore, in NDFO, the G-type ordering of rare-earth moments is as likely to occur as that of C type. From our neutron-diffraction measurements discussed above, we have observed C-type ordering of rare-earth. To support our experimental findings, we have performed the self-consistent total energy calculations within GGA+ U approximation for both C-type (experimentally observed one) and G-type orders of the rare-earth moments, keeping the Fe moments in G-type order. We observe from our calculations that for both structural arrangements (111 and 001) of Nd and Dy, C-type magnetic order emerges as the lowest energy state which is consistent with our neutron-diffraction results. The relative energies are listed in Table II wherein the C-type ordering is set to 0 meV. As seen for the alternate arrangement of Nd/Dy atoms, the G-type ordering has a higher energy as compared to the layered arrangement. Thus it is established from our experimental observations as well as our DFT calculations that the rare-earth ions order in C-type AFM in NDFO.

The most difficult part to probe is the spin-reorientation behavior of the Fe^{3+} moments. To understand the role of anisotropy and the $\Gamma_4 \rightarrow \Gamma_2$ spin reorientation in NDFO, noncollinear calculations, with spin-orbit coupling within GGA+ U +SO approximation, are performed for relaxed structural parameters corresponding to 300 K and 1.5 K. These calculations are performed only for the case of (111) arrangement of the Nd/Dy atoms as this arrangement is found to be lower in energy than the (001) arrangement. As $R^{3+} - \text{Fe}^{3+}$ interactions are nearly an order of magnitude smaller than

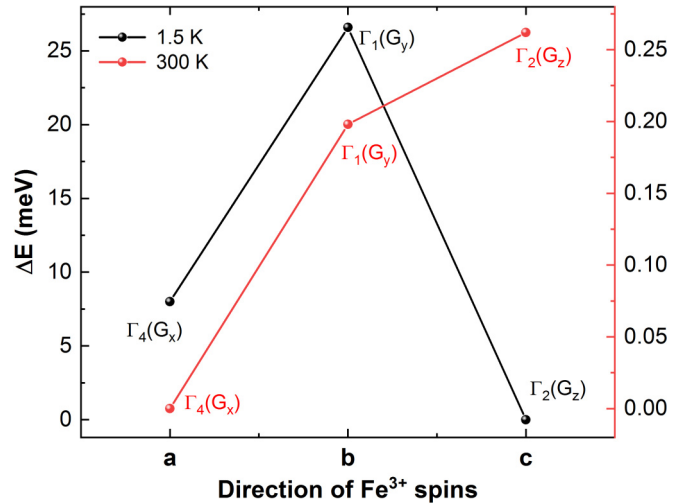


FIG. 10. Relative energies (in meV per unit cell) calculated from noncollinear calculations within GGA+ U +SO for Fe^{3+} spins along the three crystallographic directions for 300 K (red) and 1.5 K (black) crystal structures.

the $\text{Fe}^{3+} - \text{Fe}^{3+}$ exchange interactions, for 300 K the $4f$ electrons of Nd and Dy are considered as core electrons and thus nonmagnetic. In such a scenario, we performed calculations with Fe^{3+} moments pointing along crystallographic a , b , and c axes in G-type antiferromagnetic arrangements. The trend in relative energies from our noncollinear calculations are shown in Fig. 10. It is clearly seen that in case of 300 K structure, the magnetic order with Fe moments pointing along crystallographic a direction [$\Gamma_4(G_x)$], is the preferred one which is in agreement with our neutron data. For $T = 1.5$ K, the $4f$ electrons of Nd and Dy are considered as valence electrons with the magnetic moment fixed according to c_y^R component of Γ_2 representation. The calculations were performed for the three different directions of Fe magnetic moments corresponding to $c(\Gamma_2)$, $b(\Gamma_1)$, and $a(\Gamma_4)$ directions. From Fig. 10, we see that the $c(\Gamma_2)$ direction of Fe^{3+} has the lowest energy, indicating it to be the easy axis of Fe^{3+} spins, consistent with experimental results and symmetry analysis. On the other hand, the b direction which is the easy axis of Fe^{3+} spins in DyFeO_3 , has highest energy. Interestingly, one also observes from Fig. 10 that in the low-temperature phase, the $c(\Gamma_2)$ and $a(\Gamma_4)$ configurations are energetically closer to each other than $b(\Gamma_1)$. Whereas, in the high-temperature phase, $c(\Gamma_2)$ and $a(\Gamma_4)$ configurations are well separated in energies. This observation can be directly correlated with our neutron diffraction measurements, where it is seen that at high temperatures there exists a pure $a(\Gamma_4)$ phase whereas at low temperatures, a mixed phase of $c(\Gamma_2)$ and $a(\Gamma_4)$ emerges. This implies a significant role of Nd/Dy $4f$ states in the reappearance of $a(\Gamma_4)$ phase at low temperatures. To establish the exact ground-state magnetic order, we have calculated the total energy of the mixed phase [considering 50% $c(\Gamma_2)$ and 50% $a(\Gamma_4)$], where Fe spins point along 45° in the ac plane (see Fig. 11). We observe that this phase is lower in energy by about 23 meV with respect to that of the pure $c(\Gamma_2)$ phase. Therefore, this mixed phase with Fe spins canted in the ac plane is indeed the true ground-state magnetic structure of

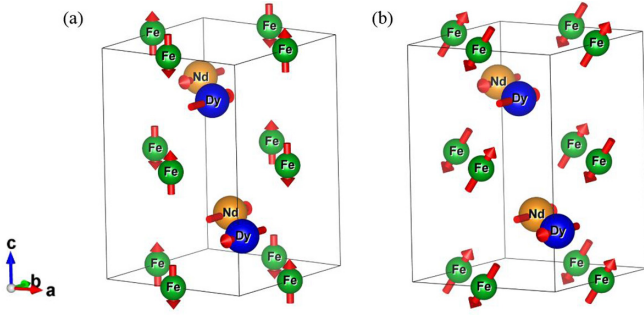


FIG. 11. Magnetic structures of NDFO in (a) Γ_2 phase and (b) mixed phase of Γ_2 and Γ_4 with Fe spins canted in the ac plane considered in our calculations. As shown in (b), the mixed phase is observed to be the ground state.

NDFO, as also observed in our neutron-diffraction experiments.

In the orthoferrites, below the spin-reorientation temperature, the $R^{3+}-R^{3+}$ exchange interactions compete with the $R^{3+}-Fe^{3+}$ exchange interactions. In the Nd-based isostructural compounds where the B-site atom is nonmagnetic, for instance, $NdGaO_3$ and $NdScO_3$, the Nd^{3+} moments order as G-type [51,52]. The highly anisotropic $Nd^{3+}-Cr^{3+}$ exchange interactions in $NdCrO_3$, though polarizing the Nd^{3+} moments, clearly affect and eventually suppress the Nd^{3+} ordering [18]. Similarly, in $NdFeO_3$, $Nd^{3+}-Fe^{3+}$ exchange interactions cause polarization of the Nd^{3+} moments, which thereby order as c_y^R , shifting the Nd^{3+} ordering to $T_{N2} \sim 1.05$ K. On the other hand, in $DyFeO_3$, the Dy^{3+} moments order independently as (g_x^R, a_y^R) , indicating negligible polarization of Dy^{3+} due to Fe^{3+} moments. Thus in NDFO, it would be interesting to obtain an idea of the order of various exchange interactions as the $Nd^{3+}-Fe^{3+}$ anisotropic exchange interactions seem to play a much larger role compared to the large single ion anisotropy of Dy^{3+} ion and the $Dy^{3+}-Dy^{3+}$ interactions. We have determined the strengths of the $Nd^{3+}-Nd^{3+}$, $Dy^{3+}-Dy^{3+}$, and $Nd^{3+}-Dy^{3+}$ exchange interactions within the GGA+ U approximation ($U_{\text{eff}} = 6$ eV). Additionally, the strength of $Nd^{3+}/Dy^{3+}-Fe^{3+}$ exchange interactions are also determined. The exchange interaction strengths are evaluated by mapping the energy difference between the ferromagnetic and antiferromagnetic configurations to the Heisenberg spin Hamiltonian as per the method used by Weingart *et al.* [53].

The calculations were performed on ‘‘artificial unit cells’’ in which, except for the selected Fe or Nd/Dy atoms, the rest of the magnetic atoms were replaced by nonmagnetic atoms. Thus, the Fe atom is replaced by Al, while Nd and Dy are replaced by La atoms. The Al^{3+} and La^{3+} ions are nonmagnetic. The interaction strengths (J) are determined between the pair of atoms that are (a) in ab plane and (b) out of plane along the c direction and are listed in Table III. The $Fe^{3+}-Fe^{3+}$ interaction which is strongest is antiferromagnetic in-plane and out-of-plane, corresponding to the G-type magnetic ordering. The highly isotropic nature is seen from the small difference between J_{ab} and J_c . Compared to $Fe^{3+}-Fe^{3+}$, rest of the interactions are nearly an order of magnitude smaller. The interaction strength between $Nd^{3+}-Fe^{3+}$ has the second high-

TABLE III. In-plane (ab) and out-of-plane (along c) exchange interaction strength (J) between the R^{3+} and Fe^{3+} in NDFO. + sign corresponds to AFM, while ‘-’ sign corresponds to FM interactions.

Exchange Interaction	J_{ab} (meV)	J_c (meV)
$Nd^{3+}-Nd^{3+}$	-0.028	-0.40
$Dy^{3+}-Dy^{3+}$	-0.31	-1.8
$Nd^{3+}-Dy^{3+}$	0.40	-0.31
$Nd^{3+}-Fe^{3+}$	-0.62	-0.68
$Dy^{3+}-Fe^{3+}$	0.015	0.020
$Fe^{3+}-Fe^{3+}$	5.40	5.28

est value which determines the magnetic ordering of the R^{3+} moments below the reorientation region. On the other hand, the $Dy^{3+}-Fe^{3+}$ exchange interaction is the weakest. This is in agreement with the previous experimental studies which show that the $Dy^{3+}-Fe^{3+}$ exchange field in $DyFeO_3$ is ~ 2 T [54], while in $NdFeO_3$, the $Nd^{3+}-Fe^{3+}$ exchange field is nearly 6.6 T [17]. The $Nd^{3+}-Nd^{3+}$ and $Dy^{3+}-Dy^{3+}$ exchange interactions are highly anisotropic. The magnitude of the latter is considerably higher along the c direction, which is expected since the Dy^{3+} moments in the parent compound $DyFeO_3$ order nearly at 4.5 K. However in NDFO, 50% substitution by Nd tends to suppress the $Dy^{3+}-Dy^{3+}$ interactions. Most importantly, the nature of $Nd^{3+}-Dy^{3+}$ exchange interaction is clearly C-type with opposite signs for in-plane (AFM) and out-of-plane (FM) interactions. Moreover, the competing exchange interaction strengths of $Nd^{3+}-Dy^{3+}$, $Nd^{3+}-Fe^{3+}$ evidently play a major role in driving the spin-reorientation of Fe moments at low temperatures. Note that even though $R^{3+}-R^{3+}$ exchange interaction strengths are much weaker than $R^{3+}-Fe^{3+}$ or $Fe^{3+}-Fe^{3+}$ exchange interaction strengths, these are an order of magnitude higher than the corresponding dipolar exchange interactions between rare-earth ions.

To correlate the various exchange interactions estimated from DFT (see Table III) with the magnetic and spin-reorientation transitions observed in the experiments, we have performed mean-field calculations on a Heisenberg spin Hamiltonian considering a simple cubic arrangement for Fe sublattices. We have considered three cases where the molecular exchange field experienced by the Fe sublattice originates from (i) the $Fe^{3+}-Fe^{3+}$ exchange, which is responsible for high temperature paramagnetic to G-type AFM transition, (ii) the $Nd^{3+}/Dy^{3+}-Fe^{3+}$ exchange, which is believed to be responsible for the first reorientation transition of Fe^{3+} spins around 75 K, and (iii) $Nd^{3+}-Dy^{3+}$ exchange, which results in an effective molecular field responsible for the second reorientation transition of Fe^{3+} spins around 10 K. In Fig. 12, the temperature dependence of Fe sublattice magnetization is presented using the respective exchange interactions from Table III. Though mean-field approximation is known to overestimate the transition temperatures, the order of all three transition temperatures are clearly consistent with those observed in the experiment, which further establishes the role of various exchange interactions in spin-reorientation transitions.

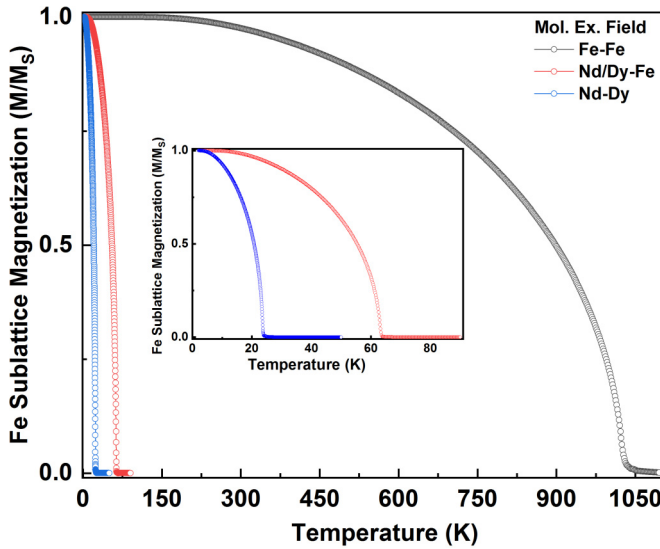


FIG. 12. Temperature dependence of Fe sublattice magnetization under molecular exchange field provided by Fe-Fe exchange (gray), Nd/Dy-Fe exchange (red), and Nd-Dy exchange (blue). Next-nearest-neighbor Fe-Fe exchange of -0.143 meV is included in addition to the near-neighbor exchange interactions given in Table III. The Nd-Dy exchange field was considered along b direction only as Nd/Dy order in c_y configuration.

V. DISCUSSION

In NdFeO₃, the anisotropic nature of Nd³⁺–Fe³⁺ exchange interactions causes the $\Gamma_4 \rightarrow \Gamma_2$ reorientation of the Fe³⁺ spins in the temperature range 200–105 K. In NDFO, these interactions are greatly diluted due to the Dy³⁺ ions which cause the reorientation to start below 75 K. In the reorientation region, effective molecular fields arise in the a - c plane and act on the magnetic moments of Fe³⁺ and the rare-earth ions. The effective field $\mathbf{H}_{\text{Nd-Fe}}$, arising due to the Nd³⁺–Fe³⁺ interactions, eventually results in (f_x^R, c_y^R) polarization of the Nd³⁺ moments [11]. Due to comparatively weaker Dy³⁺–Fe³⁺ exchange interactions in NDFO, the extent of Dy³⁺ polarization is expected to be smaller in comparison to that of the Nd³⁺ moments.

Below 25 K, the Nd³⁺ moments of NdFeO₃ start to polarize in c_y^R configuration [17]. A similar kind of polarization also occurs in NDFO. The ordering c_y^R results in development of the y component of $\mathbf{H}_{\text{Nd-Fe}}$, corresponding to the effective field in the b direction, wherein the sign is alternate on each Fe³⁺ ion. In NDFO, the y component of $\mathbf{H}_{\text{Nd-Fe}}$ can induce additional reorientation of the Fe³⁺ spins towards the Γ_4 phase. Moreover, the noncollinear calculations show that Γ_2 and Γ_4 phases are energetically very close to each other. Thus even small effective fields can result in the re-emergence of the Γ_4 magnetic structure of the Fe³⁺ spins. Therefore, the Fe³⁺ spins show an additional spin reorientation between 10–15 K. As a result, the magnetic structure of Fe³⁺ spins in NDFO is given by $\Gamma_{2+4}(\Gamma_2+\Gamma_4)$ representation at low temperatures (<10 K).

In NDFO, the (100) peak associated with long-range c_y^R ordering of the rare-earth ions is observed only from 3.5 K onward. The same peak in NdFeO₃ is observed below 25 K.

The lower ordering temperature in case of NDFO might be due to the lower strength of the Dy³⁺–Fe³⁺ interaction. Interestingly the R^{3+} ordering, in NDFO, shows a greater magnetic moment of $1.8 \mu_B$, indicating a partial polarization of Dy³⁺ moments as well. Enhanced magnetic moment of rare-earth ions is attributed to Nd³⁺–Dy³⁺ interactions. Also, due to crystal-field effects in Nd³⁺ and Dy³⁺ (Kramer’s ions), a large difference between the effective magnetic moments of both ions occurs. The Nd³⁺ ion has a moment in the range ~ 0.9 - $1 \mu_B$, while the Dy³⁺ ion has a moment of nearly $9 \mu_B$ [17,22]. Thus, the effective field can induce polarization of the large Dy³⁺ moments also in the (f_x^R, c_y^R) configuration.

In DyFeO₃, as magnetic field along the b direction results in the development of Γ_4 structure, the Dy³⁺ moments undergo a reorientation to (c_x^R, f_y^R) [55]. However, a signature of (001) magnetic Bragg peak is not observed in NDFO, which corresponds exclusively to c_x^R .

Finally, we discuss the possibility of magnetoelectric effect in NDFO. In NdFeO₃, the magnetic point group $D_{2h}(C_{2h})m'm'm$ possesses inversion symmetry. As a result, its magnetoelectric tensor is zero. In DyFeO₃, the $\Gamma_5(g_x^R, a_y^R)$ magnetic structure of Dy³⁺ belongs to the magnetic point group $D_{2h}(D_2)m'm'm'$ which has nonzero diagonal elements in the magnetoelectric tensor [12,56]. Below T_{N2} , the magnetic structure of Fe³⁺/Dy³⁺, with $\Gamma_{15}(A_x, G_y, C_z; g_x^R, a_y^R)$ representation, has a polar magnetic point group $D_2(D_2)222$, which is responsible for a nonzero magnetoelectric tensor (α_{zz}) [12]. The magnetic point group of NDFO, corresponding to Γ_{24} representation, is $C_{2h}(C_i)2m'$ which is a non-polar point group and hence does not possess any magnetoelectric coupling terms due to inversion symmetry [12]. Thus the magnetic structure of NDFO does not lead to magnetoelectric effect. From our structural studies, we do not obtain reduction in structural symmetry which can result in ferroelectric polarization. The absence of magnetoelectric effect is also confirmed from dielectric measurements in the presence of magnetic field up to 5 T (data not shown).

VI. SUMMARY AND CONCLUSIONS

To summarize, NDFO polycrystalline samples were studied in detail to understand their complex magnetic and electronic properties. The material crystallizes in the space group $Pbnm$ with both Nd and Dy, occupying the same crystallographic position and thus being randomly distributed in the crystal. Though the magnetic properties of NDFO are similar to that of NdFeO₃, there are many interesting and significant differences between the two. Below T_{N1} (~ 700 K), magnetic structure belongs to $\Gamma_4(G_x, F_z)$ representation, with the a axis being the easy axis of the Fe³⁺ magnetic moments. The large single anisotropy of Dy³⁺ which induces an abrupt $\Gamma_4 \rightarrow \Gamma_1$ spin reorientation in DyFeO₃ is suppressed with 50% Nd substitution. Instead, a gradual $\Gamma_4 \rightarrow \Gamma_2$ reorientation of the Fe³⁺ spins is observed which begins close to 75 K and results in a magnetic structure represented by $\Gamma_2(F_x, G_z)$ at 20 K with the c axis as the easy axis. Interestingly, the magnetic structure given by Γ_4 re-emerges again below 10 K.

This also coincides with the development of (100) magnetic Bragg peak which corresponds to the c_y^R arrangement of the Nd³⁺/Dy³⁺ magnetic moments. This is unlike the

G-type (g_x^R) magnetic ordering associated usually with Dy^{3+} moments. The symmetry of the rare-earth ordering also does not support any magnetoelectric coupling, which is also confirmed from field-dependent dielectric measurements.

At 1.5 K, the rare-earth ordering results in a magnetic moment of $1.8 \mu_B$ which is lower than the expected average magnetic moment of $\sim 5 \mu_B$ from $\text{Nd}^{3+}/\text{Dy}^{3+}$ magnetic sublattice, but the observed value ($1.8 \mu_B$) is much higher than the experimentally observed moments from Nd ordering in NdFeO_3 . The complete absence of a λ anomaly in specific heat clearly indicates that the ordering of $\text{Nd}^{3+}/\text{Dy}^{3+}$ moments is induced by effective molecular fields arising due to Fe^{3+} spins. The process of reorientation and rare-earth ordering is explained by our first-principles DFT calculations, considering both collinear and noncollinear spin arrangements within GGA+ U +SO approximation. The rare-earth ordering clearly shows a preference of C-type over G-type ordering. The noncollinear spin calculations show that the Fe^{3+} spins prefer to align as G_z which is symmetry compatible with the c_y^R arrangement of the Nd/Dy moments. The mixed phase of Γ_2 and Γ_4 with Fe^{3+} moments canted in the ac plane is found

to be the ground state of NDFO from our DFT calculations. The various “bare-exchange” interactions obtained for simplified unit cells show that while the $\text{Dy}^{3+}-\text{Fe}^{3+}$ interaction is weakest, the $\text{Nd}^{3+}-\text{Fe}^{3+}$ and $\text{Nd}^{3+}-\text{Dy}^{3+}$ interactions compete with the $\text{Dy}^{3+}-\text{Dy}^{3+}$ interactions, which leads to the strong polarization of the rare-earth ($\text{Nd}^{3+}/\text{Dy}^{3+}$) sublattice. It can be concluded that due to the highly unequal magnetic moments of the rare-earth ions, a molecular field acts on the R as well as the Fe^{3+} moments. The net field can lead to a successive $\Gamma_2 \rightarrow \Gamma_4$ spin reorientation of the Fe^{3+} spins.

ACKNOWLEDGMENTS

This work was supported by the UGC-DAE Consortium for Scientific Research (CSR) and Science and Engineering Research Board (SERB) through CRS-M-228, ECR/2015/000136, respectively. We acknowledge the support from IIT Roorkee through SMILE-13 grant. A.S. and S.R. acknowledge MHRD for research fellowships. M.A. acknowledges UGC-DAE Consortium for Scientific Research (CSR) through CRS-M-228 for research fellowship.

-
- [1] Y. Tokunaga, S. Iguchi, T. Arima, and Y. Tokura, *Phys. Rev. Lett.* **101**, 097205 (2008).
- [2] G. Deng, P. Guo, W. Ren, S. Cao, H. E. Maynard-Casely, M. Avdeev, and G. J. McIntyre, *J. Appl. Phys.* **117**, 164105 (2015).
- [3] Y. Du, Z. X. Cheng, X. L. Wang, and S. X. Dou, *J. Appl. Phys.* **107**, 09D908 (2010).
- [4] A. Stroppa, M. Marsman, G. Kresse, and S. Picozzi, *New J. Phys.* **12**, 093026 (2010).
- [5] A. V. Kimel, A. Kirilyuk, A. Tsvetkov, R. V. Pisarev, and Th. Rasing, *Nature* **429**, 850 (2004).
- [6] J. A. de Jong, A. V. Kimel, R. V. Pisarev, A. Kirilyuk, and Th. Rasing, *Phys. Rev. B* **84**, 104421 (2011).
- [7] P. Mandal, V. S. Bhadram, Y. Sundarayya, C. Narayana, A. Sundaresan, and C. N. R. Rao, *Phys. Rev. Lett.* **107**, 137202 (2011).
- [8] E. Pavarini and E. Koch, *Phys. Rev. Lett.* **104**, 086402 (2010).
- [9] F.-K. Chiang, M.-W. Chu, F. C. Chou, H. T. Jeng, H. S. Sheu, F. R. Chen, and C. H. Chen, *Phys. Rev. B* **83**, 245105 (2011).
- [10] W. Sławiński, R. Przeniosło, I. Sosnowska, and E. Suard, *J. Phys.: Condens. Matter* **17**, 4605 (2005).
- [11] T. Yamaguchi, *J. Phys. Chem. Solids* **35**, 479 (1974).
- [12] T. Yamaguchi and K. Tsushima, *Phys. Rev. B* **8**, 5187 (1973).
- [13] S. J. Yuan, W. Ren, F. Hong, Y. B. Wang, J. C. Zhang, L. Bellaiche, S. X. Cao, and G. Cao, *Phys. Rev. B* **87**, 184405 (2013).
- [14] G. Gorodetsky, R. M. Hornreich, I. Yaeger, H. Pinto, G. Shachar, and H. Shaked, *Phys. Rev. B* **8**, 3398 (1973).
- [15] J. Wang, J. Liu, J. Sheng, W. Luo, F. Ye, Z. Zhao, X. Sun, S. A. Danilkin, G. Deng, and W. Bao, *Phys. Rev. B* **93**, 140403(R) (2016).
- [16] E. Constable, D. L. Cortie, J. Horvat, R. A. Lewis, Z. Cheng, G. Deng, S. Cao, S. Yuan, and G. Ma, *Phys. Rev. B* **90**, 054413 (2014).
- [17] J. Bartolomé, E. Palacios, M. D. Kuz'min, F. Bartolomé, I. Sosnowska, R. Przeniosło, R. Sonntag, and M. M. Lukina, *Phys. Rev. B* **55**, 11432 (1997).
- [18] F. Bartolomé, M. D. Kuz'min, J. Bartolomé, J. Blasco, J. Garcia, and F. Sapiña, *Solid State Commun.* **91**, 177 (1994).
- [19] P. Pataud and J. Sivardière, *J. Phys. (France)* **31**, 1017 (1970).
- [20] G. Gorodetsky, B. Sharon, and S. Shtrikman, *J. Appl. Phys.* **39**, 1371 (1968).
- [21] L. A. Prelorendjo, C. E. Johnson, M. F. Thomas, and B. M. Wanklyn, *J. Phys. C: Solid St. Phys* **13**, 2567 (1980).
- [22] L. M. Holmes, L. G. V. Uitert, R. R. Hecker, and G. W. Hull, *Phys. Rev. B* **5**, 138 (1972).
- [23] L. S. Wu, S. E. Nikitin, M. Frontzek, A. I. Kolesnikov, G. Ehlers, M. D. Lumsden, K. A. Shaykhutdinov, E. J. Guo, A. T. Savici, Z. Gai, A. S. Sefat, and A. Podlesnyak, *Phys. Rev. B* **96**, 144407 (2017).
- [24] Z. Y. Zhao, X. Zhao, H. D. Zhou, F. B. Zhang, Q. J. Li, C. Fan, X. F. Sun, and X. G. Li, *Phys. Rev. B* **89**, 224405 (2014).
- [25] R. M. Hornreich, Y. Komet, R. Nolan, B. M. Wanklyn, and I. Yaeger, *Phys. Rev. B* **12**, 5094 (1975).
- [26] H. Schuchert, S. Hüfner, and R. Faulhaber, *J. Appl. Phys.* **39**, 1137 (1968).
- [27] H.-R. Fuh, K.-C. Weng, Y.-P. Liu, and Y.-K. Wang, *J. Alloys Compd.* **622**, 657 (2015).
- [28] W. Wang, W. Feng, J. Yuan, N. Pang, X. Zhao, M. Li, Z. Bao, K. Zhu, and D. Odkhuu, *Phys. B: Condens. Matter* **540**, 33 (2018).
- [29] J. Navarro, C. Frontera, L. Balcells, B. Martínez, and J. Fontcuberta, *Phys. Rev. B* **64**, 092411 (2001).
- [30] R. C. Sahoo, Y. Takeuchi, A. Ohtomo, and Z. Hossain, *Phys. Rev. B* **100**, 214436 (2019).
- [31] G. R. Haripriya, C. M. N. Kumar, R. Pradheesh, L. M. Martinez, C. L. Saiz, S. R. Singamaneni, T. Chatterji, V. Sankaranarayanan, K. Sethupathi, B. Kiefer, and H. S. Nair, *Phys. Rev. B* **99**, 184411 (2019).
- [32] T. Chatterji, B. Frick, M. Zamponi, M. Appel, H. S. Nair, R. Pradheesh, G. R. Haripriya, V. Sankaranarayanan, and K. Sethupathi, *Phys. Rev. B* **98**, 094429 (2018).

- [33] H.-R. Fuh, K.-C. Weng, C.-R. Chang, and Y.-K. Wang, *J. Appl. Phys.* **117**, 17B902 (2015).
- [34] A. P. G. Rodrigues, M. A. Morales, R. B. Silva, D. R. A. B. Lima, R. L. B. A. Medeiros, J. H. Araújo, and D. M. A. Melo, *J. Phys. Chem. Solids* **141**, 109334 (2020).
- [35] A. Singh, A. Jain, A. Ray, B. Padmanabhan, R. Yadav, V. Nassif, S. Husain, S. M. Yusuf, T. Maitra, and V. K. Malik, *Phys. Rev. B* **96**, 144420 (2017).
- [36] Y. Tokunaga, Y. Taguchi, T. Arima, and Y. Tokura, *Phys. Rev. Lett.* **112**, 037203 (2014).
- [37] T. Chakraborty and S. Elizabeth, *J. Magn. Magn. Mater.* **462**, 78 (2018).
- [38] H. Wu, S. Cao, M. Liu, Y. Cao, B. Kang, J. Zhang, and W. Ren, *Phys. Rev. B* **90**, 144415 (2014).
- [39] E. Li, Z. Feng, B. Kang, J. Zhang, W. Ren, and S. Cao, *J. Alloys Compd.* **811**, 152043 (2019).
- [40] J. Rodríguez-Carvajal, *Physica B (Amsterdam)* **192**, 55 (1993).
- [41] H. M. Rietveld, *J. Appl. Crystallogr.* **2**, 65 (1969).
- [42] E. Hovestreydt, M. Aroyo, S. Sattler, and H. Wondratschek, *J. Appl. Crystallogr.* **25**, 544 (1992).
- [43] G. Kresse and J. Furthmüller, *Phys. Rev. B* **54**, 11169 (1996).
- [44] J. P. Perdew, K. Burke, and M. Ernzerhof, *Phys. Rev. Lett.* **77**, 3865 (1996).
- [45] V. I. Anisimov, I. V. Solovyev, M. A. Korotin, M. T. Czyżyk, and G. A. Sawatzky, *Phys. Rev. B* **48**, 16929 (1993).
- [46] A. Singh, S. Rajput, B. Padmanabhan, K. Kaushik, M. Anas, T. Maitra, and V. K. Malik, *J. Phys.: Condens. Matter* **31**, 355802 (2019).
- [47] E. F. Bertaut, *Magnetism III*, edited by G. T. Rado and H. Suhl (Academic Press, New York, 1963).
- [48] C. M. N. Kumar, Y. Xiao, H. S. Nair, J. Voigt, B. Schmitz, T. Chatterji, N. H. Jalarvo, and Th. Brückel, *J. Phys.: Condens. Matter* **28**, 476001 (2016).
- [49] L. Chen, T. Li, S. Cao, S. Yuan, F. Hong, and J. Zhang, *J. Appl. Phys.* **111**, 103905 (2012).
- [50] R. Przeniosło, I. Sosnowska, and P. Fischer, *J. Magn. Magn. Mater.* **140-144**, 2153 (1995).
- [51] F. Luis, M. D. Kuz'min, F. Bartolomé, V. M. Orera, J. Bartolomé, M. Artigas, and J. Rubín, *Phys. Rev. B* **58**, 798 (1998).
- [52] I. Plaza, E. Palacios, J. Bartolomé, S. Rosenkranz, C. Ritter, and A. Furrer, *Physica B* **234-236**, 635 (1997).
- [53] C. Weingart, N. Spaldin, and E. Bousquet, *Phys. Rev. B* **86**, 094413 (2012).
- [54] A. K. Zvezdin and V. M. Matveev, *Sov. Phys. JETP* **50**, 543 (1979).
- [55] T. N. Stanislavchuk, Y. Wang, Y. Janssen, G. L. Carr, S. W. Cheong, and A. A. Sirenko, *Phys. Rev. B* **93**, 094403 (2016).
- [56] A. K. Zvezdin and A. A. Mukhin, *JETP Lett.* **88**, 505 (2009).